Local optical density of states in SiO_2 spherical microcavities: Theory and experiment

M. J. A. de Dood, L. H. Slooff, and A. Polman
FOM Institute for Atomic and Molecular Physics, Kruislaan 407, 1098 SJ Amsterdam, The Netherlands

A. Moroz* and A. van Blaaderen
FOM Institute for Atomic and Molecular Physics, Kruislaan 407, 1098 SJ Amsterdam, The Netherlands
and Condensed Matter Department, Debye Institute, Utrecht University,
P.O. Box 80000, 3508 TA Utrecht, The Netherlands

(Received 7 February 2001; published 13 August 2001)

The local optical density of states (LDOS) in 340-nm-diam SiO_2 spherical microcavities was calculated and probed experimentally by measuring the luminescence decay rate at 1.54 μm of erbium ions implanted in the colloids. To separate the effect of nonradiative processes, first the radiative decay rate of Er^{3+} in bulk SiO_2 was determined. This was done by varying the LDOS in an Er-doped planar SiO_2 film by bringing the film into contact with liquids of different refractive index in the range $n=1.33-1.57$. By comparing the calculated LDOS with the observed changes in decay rate with index, the radiative rate was found to be $54\pm10\,s^{-1}$ ($\tau=18\pm3$ ms) in bulk SiO_2. This value was then used to analyze the difference in decay rate in colloids surrounded by air or immersed in an index-matching liquid. Within the experimental error, agreement was found between the calculated and experimentally probed LDOS in the colloids. Finally, a full determination of the LDOS vs size in SiO_2 microcavities is presented ($2\pi R/\lambda=0.1-6.9$), which shows the appearance of a number of maxima, corresponding to the position of the electric-type resonances inside the microcavity.

DOI: 10.1103/PhysRevA.64.033807 PACS number(s): 42.50.−p, 12.20.Fv, 68.55.Ln, 42.70.Ce

I. INTRODUCTION

The spontaneous-emission rate of an atom is not a property of the atom only, but depends on the local optical surrounding as well. Recently, there has been a growing interest in the use of dielectric structures, such as microcavities and photonic band-gap materials, to modify the rate of spontaneous emission. Such modifications were observed for Rydberg atoms [1,2], for atoms placed in microcavities [3–5], in thin films [6], close to a mirror or dielectric interface [7–10], in liquid microdroplets [11–13], and photonic crystals [14–16].

The changes in decay rate can be determined by calculating the local density of states (LDOS) and then applying Fermi's Golden Rule to obtain the radiative decay rate. It has been shown that the radiative decay rate is proportional to this LDOS, both in a scalar approximation [17] and for the full Maxwell equations [18,19]. For relatively simple geometries, the LDOS can be calculated using either a full set of eigenfunctions of the Helmholtz wave equation [20–22] or by using Green's functions [23,24].

Luminescent ions can be used to experimentally probe the LDOS. In general, the measured changes in decay rate cannot be compared directly to theoretical results because nonradiative processes that occur parallel to the radiative decay must be taken into account. Therefore, in an experimental determination of the LDOS, accurate and reproducible methods are needed so that the nonradiative and radiative decay rates can be determined independently.

Trivalent rare-earth ions are excellent candidates to probe the LDOS, since the optical transitions occur in the visible and near-infrared part of the spectrum and they have excited-state lifetimes in the millisecond range with high quantum efficiencies [7,9,25]. The transition frequency is almost insensitive to the host material and resembles that of the free ion, due to the fact that the optical transitions take place in the $4f$ shells that are shielded from interactions with the host material by the $5s$ and $5p$ electrons. Ion implantation of rare-earth elements can be used to put the atoms at a well-defined depth in almost any host material [26].

In this paper, we study the radiative decay rate of optically active Er^{3+} ions incorporated in SiO_2 colloidal spheres, which serve as small spherical microcavities. To separate radiative and nonradiative components in the decay, experiments were also done on an erbium-implanted SiO_2 thin film on a silicon substrate. By changing the LDOS in the film by bringing it in contact with liquids with different refractive indices, and monitoring the change in the decay rate of the erbium ions, the radiative and nonradiative decay rates of Er^{3+} ions in bulk SiO_2 were determined. This resulted in the first experimental determination of the radiative decay rate of Er^{3+} in pure SiO_2. These data were then used to analyze experimentally observed changes in decay rate for Er^{3+}-doped SiO_2 colloids upon immersing the colloids in an index-matching liquid. A large effect is observed if the Er^{3+} is incorporated in a 340-nm-diam spherical microcavity, which can be attributed to the geometry of the microcavity.

II. EXPERIMENT

SiO_2 colloidal spheres were made using a wet chemical reaction from tetra-ethoxy-silane (TEOS), ethanol, ammonia, and water. The sphere diameter obtained was 340 nm at a size polydispersity of 5%. The colloids were deposited on Si(100) substrates that were cleaned for 15 min in a 1.0-M

*On leave of absence from the Institute of Physics, AS CR, Na Slovance 2, Prague, Czech Republic.

KOH solution in ethanol and rinsed in pure ethanol before use. A droplet of the spheres dissolved in ethanol was put on the substrate, and the ethanol was allowed to evaporate, leading to the formation of three to four layers of stacked spheres.

A SiO_2 layer of 100-nm thickness was grown on a Si(100) substrate in two consecutive steps using a reaction mixture of TEOS, ethanol, ammonia, and water. The substrates were put into the reaction mixture and the layer was grown for 2 h under continuous stirring of the mixture. Details of the synthesis procedure and characterization of the layers and the spheres are published elsewhere [27–31].

The 100-nm-thick SiO_2 film was implanted with 70-keV Er^+ ions to fluences of 3.4×10^{14} ions/cm^2 and 9.1×10^{14} ions/cm^2 at room temperature. The 340-nm-diam spheres were implanted with 350-keV Er^+ ions to fluences of 0.9×10^{15} and 2.5×10^{15} at cm^{-2}. Both implantation conditions were chosen to lead to the same nominal Er peak concentrations of 0.2 and 0.5 at. %. After implantation, all samples were annealed in a vacuum furnace (pressure $\leqslant 5\times10^{-7}$ mbar) at 100 °C for 1 h and at 900 °C for 1 h.

Scanning electron microscopy (SEM) images of the colloids were taken using 5-keV electrons at a resolution better than 5 nm. Photoluminescence (PL) spectra were obtained using the 488-nm line of an Ar-ion laser as a pump source. The pump beam was modulated at a frequency of 13 Hz using an acousto-optic modulator. The PL signal was focused onto the entrance slits of a 96-cm grating monochromator and detected by a liquid-nitrogen-cooled Ge detector employing standard lock-in techniques. The spectral resolution of the system was 6 nm. PL decay traces of the luminescence were recorded at the peak of the Er^{3+} luminescence at 1.536 μm and averaged using a digitizing oscilloscope. The overall time response of the system was measured to be 30 μs. Transparent liquids of different refractive index ($n=1.33-1.57$) were brought into contact with the sample surface, while the luminescence signal was collected from the (unpolished) backside of the Si substrate. Since silicon is transparent for wavelengths longer than 1.1 μm, the Er^{3+} luminescence around 1.54 μm can be collected without difficulties. The pump laser beam was directed onto the sample surface through the liquid films. The liquids used in our experiments are water ($n=1.33$), a microscope immersion oil (Merck, according to DIN 58884, $n=1.51$), and iso-eugenol ($n=1.57$). An index-matching liquid ($n=1.45$) was prepared by mixing water and ethylene glycol in the right proportions.

III. RESULTS AND DISCUSSION

A. Synthesis and photoluminescence

Figure 1 shows a SEM image of the 340-nm silica colloids. A layered structure composed of three to four layers can be vaguely determined from the SEM image. The layer thickness was found more accurately in Rutherford backscattering spectrometry (RBS) measurements [25]. RBS on the SiO_2 film implanted with 70-keV Er ions shows a Gaussian Er depth distribution peaking at a depth of 39 nm with a standard deviation $\sigma=11$ nm. The peak concentrations are

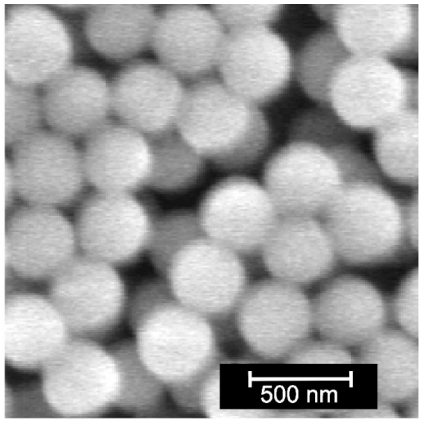

FIG. 1. SEM image of SiO_2 colloidal spheres (diameter 340 nm) deposited on a Si substrate.

0.2 and 0.5 at. %, respectively. Spectroscopic ellipsometry measurements (not shown) on the annealed Er-implanted film indicate that the SiO_2 layer thickness is 100 nm and the refractive index equals that of pure SiO_2 made by thermal oxidation ($n=1.45$).

The PL spectrum of a sample with three to four layers of 340-nm spheres annealed at 900 °C is shown in Fig. 2. The Er^{3+} ions are excited into the $^4F_{7/2}$ level as shown in the inset. The emission is due to transitions from the first excited state ($^4I_{13/2}$) to the ground state ($^4I_{15/2}$), peaking at a wavelength of 1.536 μm. Other samples, implanted to higher erbium fluences even if annealed at different temperatures, as well as the 100-nm-thick SiO_2 layers, show the same PL spectrum. This spectrum is similar to the PL spectrum of erbium ions implanted into thermally grown SiO_2 [32]. Since the shape of the PL spectrum is determined by the Stark splitting of the ground state and first excited state induced by the local environment around the atom, this suggests that the

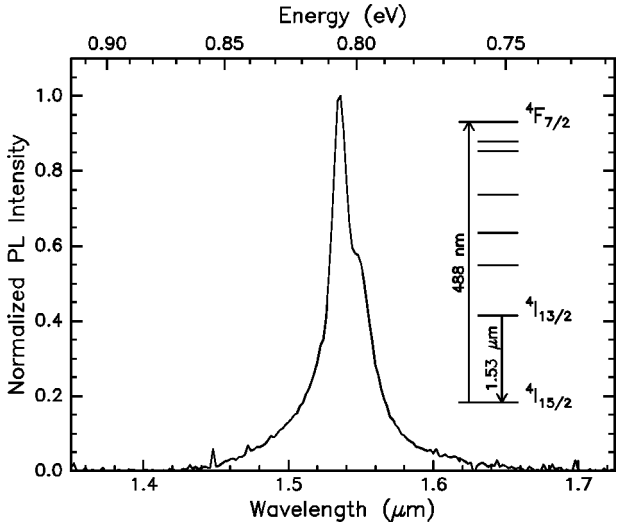

FIG. 2. PL spectrum for Er implanted SiO_2 colloids of 340 nm diameter on a silicon substrate. The 488-nm emission line from an Ar ion laser was used as an excitation source. The PL spectrum peaks at a wavelength of 1.536 μm corresponding to the $^4I_{13/2}\rightarrow{}^4I_{15/2}$ transition of Er^{3+}.

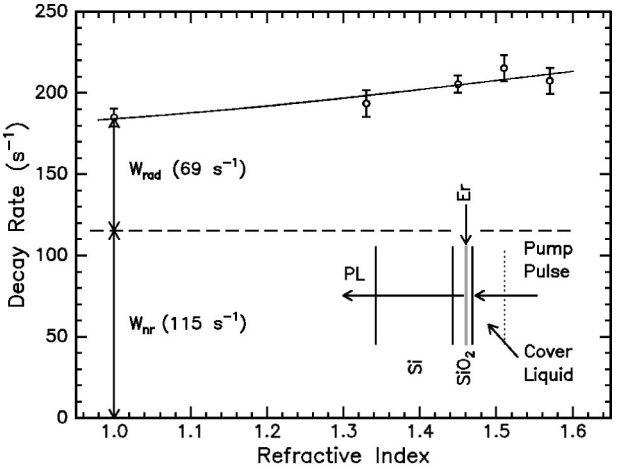

FIG. 3. Measured decay rate of Er^{3+} ions in a 100-nm-thick SiO_2 layer as a function of refractive index of the covering liquid (0.2 at. % Er). The Er^{3+} ions were excited through the liquid using the 488-nm line of an Ar-ion laser, while the PL signal was collected from the back through the Si substrate (see inset).

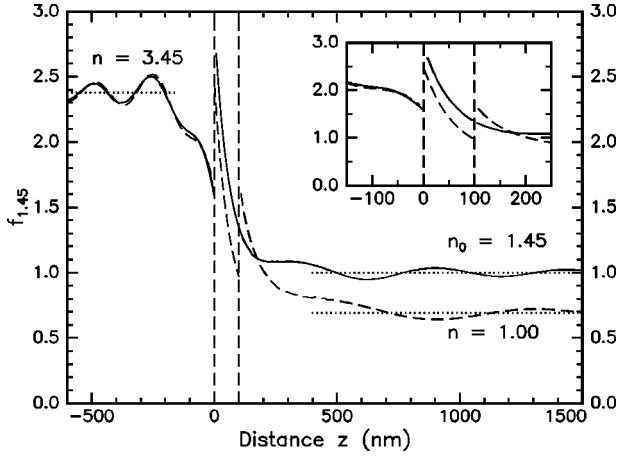

FIG. 4. Polarization- and angle-averaged local optical density of states for a 100-nm-thick SiO_2 layer ($n_0=1.45$). The layer is sandwiched between a Si substrate ($n=3.45$) and an ambient with $n=1.00$ (dashed line) or $n=n_0=1.45$ (solid line). All calculations were done for a vacuum wavelength of 1.54 μm. The inset shows the LDOS in the SiO_2 layer in more detail.

local environment of the Er^{3+} ions in all samples discussed in this paper is comparable.

In the next two sections, we will first describe experiments to determine the radiative decay rate of Er^{3+} in planar SiO_2 films and compare this value with existing literature. We will then use these data to study the LDOS in colloidal particles.

B. Luminescence lifetime and local density of states in the Er^{3+}-doped SiO_2 layer

Figure 3 shows decay rates of Er^{3+} measured at a luminescence wavelength of 1.536 μm for the SiO_2 film implanted to a peak concentration of 0.2 at. % Er. Decay rates were measured for the sample in air and in contact with liquids with refractive indices n of 1.33, 1.45 (index-matching case), 1.51, and 1.57. A clear increase of the decay rate from 184 to 205 s^{-1} is observed as the refractive index of the liquid is increased. A similar (absolute) increase in the decay rate was observed for a sample with a peak concentration of 0.5 at. % (not shown).

As we have shown before, for the simpler case of a single interface between two dielectric media of infinite thickness [9,10], the increase in decay rate with refractive index of the covering liquid can be understood by considering the optical LDOS for the SiO_2 film in contact with liquids of different refractive index. According to Fermi's Golden Rule, the radiative decay rate can be written in terms of a LDOS ρ as [9,22]

$$W_{\mathrm{rad}}(\mathbf{r})=\frac{\pi\omega}{\hbar\epsilon(\mathbf{r})}|D|^2\rho(\omega,\mathbf{r}), \tag{3.1}$$

where $\epsilon(\mathbf{r})$ is the position-dependent dielectric constant, ω is the transition frequency, and $|D|^2$ is the atomic dipole matrix element of the transition involved. This matrix element is not influenced by the optical properties of the interface. Thus the macroscopic ρ and $\epsilon(\mathbf{r})$ are the only parameters in Eq. (3.1) that are varied in our experiments.

The LDOS ρ can be calculated as a function of position $\mathbf{r}$. For a dielectric slab, this calculation is done by quantizing the electromagnetic field using a complete set of normalized eigenvectors of the classical Maxwell problem, closely following Ref. [22]. For this calculation, the complete set of incoming plane waves at a single frequency is summed, using reflection and refraction of the waves as given by the Fresnel coefficients of the layered system. Since the ions in our experiments are distributed randomly in the matrix, an integration over all angles and both polarizations was done. For an absolute determination of the radiative rate, the microscopic local field should be used in the calculation. This local field seen by the atom is due to the microscopic environment of the atom and differs from the macroscopic field. With the liquid films in our experiment, we only influence this microscopic local field through the macroscopic field since the Er^{3+} ions are relatively far away from the interface [33].

Figure 4 shows a calculation of the local LDOS $f_{1.45}$ for a 100-nm-thick SiO_2 slab ($n=1.45$) on a Si substrate ($n=3.45$) normalized to the LDOS for a bulk medium of refractive index $n=1.45$. The calculation was done for a wavelength of 1.54 μm, corresponding to the peak of the Er^{3+} emission. The factor $\epsilon(\mathbf{r})$ in Eq. (3.1) is included in the definition of $f_{1.45}$ making this LDOS directly proportional to the radiative decay rate. The position $z=0$ corresponds to the position of the Si/SiO_2 interface.

The dashed line shows the calculated LDOS for a sample in air ($n=1.00$) and the solid line shows the LDOS for an index-matched film ($n=1.45$). The oscillations in the LDOS on both sides of the interface are caused by interference between incoming and reflected waves and have a periodicity of $\sim\lambda/2n$. Such oscillations are invisible in the SiO_2 film because the film thickness is much smaller than the emission wavelength (thickness $<\lambda/4n$). Clearly, for both curves in

Fig. 4, the LDOS in the SiO_2 film is enhanced compared to that for bulk SiO_2 ($f_{1.45}=1.00$), which is due to the presence of the high-index Si substrate. The inset of Fig. 4 shows the LDOS in the SiO_2 layer in more detail, which clearly shows that the LDOS in the film increases with increasing index of the outside medium ($n=1.00-1.45$). According to Eq. (3.1), this explains the measured increase of the decay rate with refractive index as observed in Fig. 3.

The change in decay rate with refractive index can be calculated quantitatively by considering the calculated LDOS, the measured Er depth profile, and the variation of the 488-nm pump light over the film thickness due to interference. We find that the observed relative increase in decay rate is much smaller than that found in the calculation that assumes that the decay process is purely radiative. Therefore, nonradiative processes that are independent of the optical properties of the interface must be included. The total decay rate is the sum of the radiative and nonradiative decay rates:

$$W = W_{\mathrm{rad}} + W_{\mathrm{nonrad}}. \tag{3.2}$$

Using Eq. (3.1), the total decay rate can be rewritten in terms of the LDOS $f_{1.45}$:

$$W(n,z) = f_{1.45}(n,z) W_{\mathrm{rad}}^{1.45} + W_{\mathrm{nonrad}}, \tag{3.3}$$

where $f_{1.45}$ is the LDOS normalized to the LDOS in a bulk material with $n=1.45$ and $W_{\mathrm{rad}}^{1.45}$ is the radiative decay rate of Er^{3+} ions in bulk SiO_2. The solid line in Fig. 3 is a fit of Eq. (3.3) to the measured data, resulting in $W_{\mathrm{rad}}^{1.45}=54\pm10\,\mathrm{s}^{-1}$ and $W_{\mathrm{nonrad}}=115\pm10\,\mathrm{s}^{-1}$. The radiative and nonradiative rates are separated by the dashed line in Fig. 3. Note that the radiative rate for the index-matching case ($n=1.45$) is found to be $W_{\mathrm{rad}}=69\,\mathrm{s}^{-1}$ for the SiO_2 thin film. This is higher than the radiative rate in bulk SiO_2 ($54\,\mathrm{s}^{-1}$), which is due to the fact that the Er^{3+} ions are close to the high refractive index Si substrate, which enhances the radiative decay rate. Our analysis uses refractive index values n_D at $\lambda=590$ nm. As the index dispersion between 590 nm and 1.5 μm is less than 2% and the LDOS is sensitive to the difference in index between SiO_2 and the liquid, this introduces an error $<1\%$ [34].

C. Comparison with literature

The radiative rate of $54\pm10\,\mathrm{s}^{-1}$ ($\tau=18\pm3$ ms) for Er^{3+} in bulk SiO_2 found in the preceding section is identical to the lifetime measured for 10-μm-thick SiO_2 layers grown by wet thermal oxidation of Si that are implanted with 3.5-MeV Er ions [32]. In that case, the distance between the interfaces and the Er^{3+} ions is so large that the LDOS is equal to that of bulk SiO_2 within a few percent and a lifetime of 17 ms was reported ($W=59\,\mathrm{s}^{-1}$). We note that the radiative lifetime of 18 ± 3 ms determined here is larger than the lifetime found in several other studies of Er-doped SiO_2 [4,32,35] indicating that nonradiative decay plays an important role in those studies.

Our result can also be compared with measurements of the decay rate of Er^{3+} in a Si/SiO_2 planar microcavity studied by Vredenberg and co-workers in Ref. [4]. The active SiO_2 region was doped with Er^{3+} ions using Er-ion implantation. They find that the emission rate enhancement and suppression effects in such cavities are smaller than those predicted by theory. One explanation of this effect, also indicated by the authors, is that there is a nonradiative component in the decay. Using Eq. (3.3), with f equal to the cavity enhancement factor given in Fig. 3 of Ref. [4], we can fit the cavity data to Eq. (3.3) and find $W_{\mathrm{rad}}=55\,\mathrm{s}^{-1}$ and $W_{\mathrm{nonrad}}=28\,\mathrm{s}^{-1}$. This value for W_{rad} is in perfect agreement with the value obtained above for bulk SiO_2.

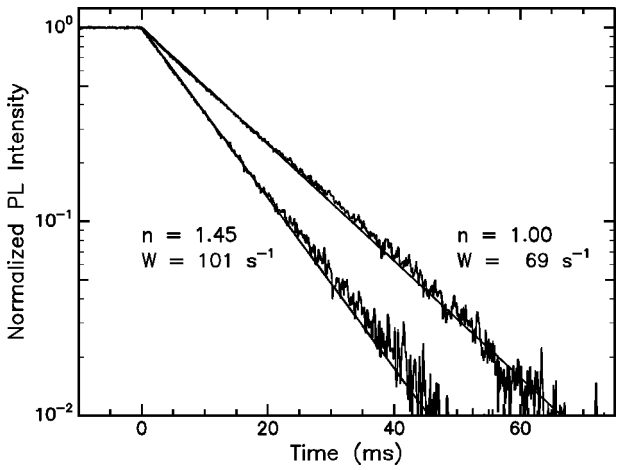

FIG. 5. Photoluminescence decay traces plotted on a logarithmic scale for erbium-ion-implanted 340-nm-diam SiO_2 spheres (0.2 at. % Er). Decay traces for the sample in air ($n=1.00$) and immersed in an index-matching liquid ($n=1.45$) are shown. The straight lines correspond to single exponential fits with decay rates of 69 and 101 s^{-1}, respectively.

The radiative rate for Er in bulk SiO_2 of 54 s^{-1} can be compared to the radiative decay rate of Er implanted in silica sodalime glass, which was determined to be 45 s^{-1} [9]. The difference is likely to be due to a difference in the local environment of the Er ions, which is also reflected in the difference in PL spectra.

D. Luminescence lifetime in Er^{3+}-doped SiO_2 spherical microcavities

Now that we have determined the radiative lifetime of Er^{3+} in bulk SiO_2, this result can be used to study changes in the luminescence lifetime of Er^{3+} in SiO_2 colloidal spheres. The SiO_2 spheres are grown using a similar process to that for the thin SiO_2 layers [31]. Therefore, the local environment is likely to be the same and hence the radiative lifetime of the Er ions is the same in both cases. Figure 5 shows Er^{3+} luminescence decay traces measured at $\lambda=1.536\,\mu$m for SiO_2 spheres of 340-nm diam (as in Fig. 1) implanted with 350-keV Er ions to a fluence of $0.9\times10^{15}\,\mathrm{ions/cm}^2$ (0.2 at. %) and annealed at 900 °C for 1 h. Two luminescence decay traces are shown: one for the spheres in air and one for the spheres in an index-matching ($n=1.45$) liquid. A large increase in the decay rate from 69 to 101 s^{-1} is observed for the index-matched case. After removing the index-matching liquid and drying the sample for several minutes, the decay rate returned to the original value of 69 s^{-1}, show-

ing that the index-matching process is reversible. We have repeated the experiment using dimethylsulfoxide (DMSO) ($n=1.48$) and fully deuterated DMSO-d6 and found the same increase by 30 s^{-1} for both cases. This excludes the possibility that the increase is due to nonradiative processes owing to $-$OH and $-$CH groups in the liquid, as the quenching rate for the two liquids should then have been very differently [36,37]. This indicates that the effect on decay rate is purely caused by the refractive index of the liquid.

In the index-matched case, the LDOS in the colloids is identical to that for the SiO_2 film on Si in contact with the index-matching liquid, as given by the solid line in Fig. 4. In the present geometry with the substrate covered with three to four layers of 340-nm spheres, the implanted Er^{3+} ions are placed 700–1000 nm away from the Si interface. As can be seen in Fig. 4, for these distances the LDOS differs by less than 7% from the bulk value. Therefore, the radiative decay rate of the Er^{3+} ions inside the index-matched spheres must be close to the rate in bulk SiO_2 of $54\pm10\,s^{-1}$. The difference with the measured rate of 101 s^{-1} is then attributed to a nonradiative decay process at a rate of 47 ± 10 s^{-1} ($101\,s^{-1}-54\,s^{-1}=47\,s^{-1}$). Having now determined the nonradiative decay rate in these colloids, we can derive the radiative decay rate in the colloids in air by subtracting the measured nonradiative rate from the measured total rate in air. This results in a radiative decay rate of $22\pm15\,s^{-1}$ ($69\,s^{-1}-47\,s^{-1}=22\,s^{-1}$) for a 340-nm-diam sphere surrounded by air.

This experimentally determined value can be compared with theoretical calculations of the LDOS for a spherical particle. The LDOS is obtained by using the imaginary part of the Green function $G(\omega;r,r)$ of the Helmholtz equation at a given frequency ω [38,39]. The LDOS is defined as [23,24,40]

$$\rho(\omega,r)=-\frac{2}{\pi}\,\mathrm{Im}\,G(\omega;r,r). \tag{3.4}$$

Using the definition of Eq. (3.4), the relation between the LDOS and the radiative decay rate is again given by Eq. (3.1).

Figure 6 shows a calculation of the LDOS for a single spherical particle at a vacuum wavelength of 1.536 μm, as a function of the radial distance, for spheres with a diameter of 175 (a), 340, (b) or 1600 nm (c). The density of states is normalized to the LDOS of a bulk medium with $n=1.45$. For the 175- and 340-nm-diam spheres, very little variation in the LDOS is observed inside the sphere. This can be explained by the fact that the emission wavelength is larger then the first Mie resonance in these spheres. Note that the average LDOS can be larger [Fig. 6(a)] or smaller [Fig. 6(b)] than the LDOS in bulk SiO_2, depending on the sphere diameter. For larger diameter spheres Mie resonances appear, leading to more pronounced variations in the LDOS as shown in Fig. 6(c) for 1600-nm spheres.

A complete representation of the LDOS for a single sphere with a refractive index $n=1.45$ surrounded by air is shown in Fig. 7, as a function of sphere diameter (horizontal axis) and the position within the sphere (vertical axis). The

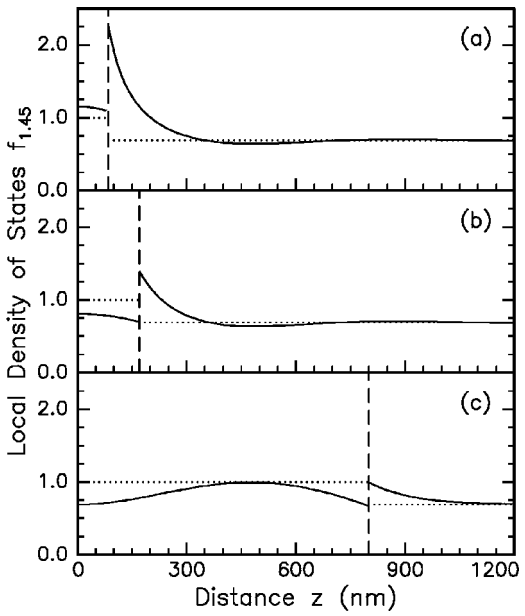

FIG. 6. Polarization- and angle-averaged LDOS as a function of radial position for a SiO_2 sphere ($n=1.45$) in air, calculated for a vacuum wavelength of 1.54 μm. Data are shown for spheres with a diameter of 175 nm (a), 340 nm (b), or 1600 nm (c).

gray scale indicates the LDOS normalized to the LDOS for bulk SiO_2 ($n=1.45$). The position within the sphere is normalized to the sphere radius such that $r/R=1$ corresponds to the edge of the sphere while $r/R=0$ corresponds to the center of the sphere. A number of maxima and minima in the LDOS are observed as a function of the sphere

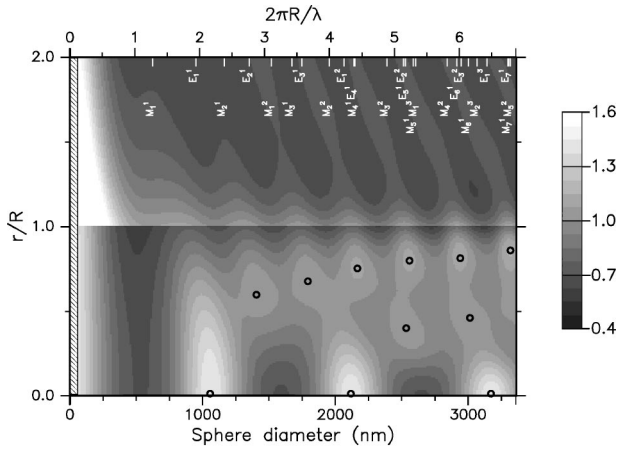

FIG. 7. Polarization- and angle-averaged LDOS for a SiO_2 sphere ($n=1.45$) in air for a vacuum wavelength of 1.536 μm as a function of normalized radial position (vertical axis) and sphere diameter (horizontal axis). The corresponding size parameter is indicated on the top axis. The LDOS is indicated by the gray scale on the right and was normalized to the density of states in bulk SiO_2. The observed maxima in the LDOS are indicated by the black dots. The positions of the magnetic and electric resonances of the sphere are indicated on the top axis. The magnetic (electric) resonance of order n is indicate by M_n^l (E_n^l), where $l=1$ corresponds to the ground tone and higher l correspond to overtones. No data were calculated in the cross-hatched region for diameters <50 nm.

TABLE I. Measured and calculated decay rates for Er^{3+}-doped SiO_2 samples (0.2 at % Er). Results are given for a 100-nm-thick SiO_2 layer and for 340-nm-diam spherical microcavities, both either in contact with air or an index-matching liquid ($n=1.45$). As discussed in the text, measurements of the decay rate in a SiO_2 film as a function of refractive index were first made (W_{exp}). From a comparison with LDOS calculations W_{rad} and W_{nonrad} were then determined for the film. The radiative rate of Er in bulk SiO_2 was then determined to be 54 s^{-1}. Next, from the measured decay rate of the index-matched spheres, the nonradiative decay rate in the colloids was found (47 s^{-1}). From this the radiative decay rate of the colloids in air was found (22 s^{-1}). The calculated radiative rate in the colloids (40 s^{-1}) was derived from a local LDOS calculation combined with the bulk radiative rate of 54 s^{-1}.

Sample	Calculated W_{rad}	W_{exp} (s^{-1})	W_{rad} (s^{-1})	W_{nonrad} (s^{-1})	QE
SiO_2 layer ($n=1.00$)	69	184	69	115	37%
SiO_2 layer ($n=1.45$)	90	205	90	115	44%
340-nm sphere ($n=1.00$)	40	69	22	47	32%
340-nm sphere ($n=1.45$)	54	101	54	47	53%

diameter, which can be compared to the position of Mie resonances or normal modes of the sphere. The positions of these resonances are indicated on the top axis. The magnetic (electric) resonance is labeled as $M_n^l(E_n^l)$, where n corresponds to the order of the resonance. $l=1$ corresponds to the ground tone of a resonance, while higher l indicate the overtones.

By comparing the position of the maxima in Fig. 7 (indicated by the black dots) with the position of the normal modes, we find that the maxima in the LDOS correspond to the position of the electric-type resonances. Depending on the order of the resonance, the maximum in the LDOS occurs in the center of the sphere or more towards the perimeter of the sphere. As can be seen in Fig. 7, the decay rate of ions placed inside a sphere can be enhanced or inhibited depending on both the sphere diameter and the position of the ions within the sphere.

The Er-doped SiO_2 spheres considered in this paper have a diameter of 340 nm, which corresponds to a size parameter that lies below the size parameter of the lowest (magnetic) normal mode of the sphere. As can be seen in Fig. 7, the LDOS is a slowly varying function of the sphere diameter in this size range. Assuming a bulk radiative rate $W_{rad}=54\pm10\,s^{-1}$, the calculation predicts a radiative decay rate in the range of $(35-40)\pm10\,s^{-1}$ depending on the distribution of the Er ions within the sphere. Within the errors, these values agree with the experimentally observed value of $22\pm15\,s^{-1}$. For small spheres, the electric field in close proximity to the sphere is enhanced due to a strong dipolar contribution. The LDOS scales with E^2, and thus strongly enhances the LDOS for small spheres [41]. Since local field effects will become important for small spheres as well, we did not perform calculations for spheres that are much smaller than those used in the experiment, corresponding to the hatched area in Fig. 7.

The measured and calculated decay rates for the SiO_2 layer and the 340-nm spheres are summarized in Table I. The quantum efficiency, defined as the ratio of the radiative rate and the total decay rate, is also indicated in Table I. Both for the film and the sphere, the quantum efficiency increases for increasing index, because of the increased relative contribution of radiative decay to the total decay. As can be seen in the table, a large difference in the nonradiative rates exists between the spheres and the layer. Since the Er concentration is 0.2 at. % in both cases, this implies that the nonradiative processes that occur in our samples depend on material properties other than the Er concentration only. One possibility is a difference in the concentration of $-$OH quenchers incorporated in the SiO_2 material that act as centers for nonradiative decay [9,42]. In this model, the large difference in quencher concentration can be explained by a difference in annealing behavior between a sphere and a thin film.

Finally we note that in our analysis we have assumed single isolated spheres. This greatly facilitates the calculation of the LDOS since the different polarizations can be treated separately. In reality, the spheres are touching and deposited on a substrate, which affects the calculated LDOS [43], and a full vector calculation of the Maxwell equations is needed. Since the error on the experimentally derived radiative decay rate in the SiO_2 colloids is rather large, we were unable to observe a significant difference between the measured data and calculations of the LDOS for an isolated sphere. Since our experiments were done on relatively small spheres compared to the emission wavelength, the effect of neighboring spheres is expected to be limited. For larger spheres, where resonances are expected, the effect of the surroundings is expected to be more pronounced, effectively spoiling the resonances observed in Fig. 7.

IV. CONCLUSIONS

The radiative decay rate for Er^{3+} implanted at a well-defined position in a SiO_2 thin film was determined by bringing it into contact with liquids of different refractive index in the range between 1.33 and 1.57. The decay rate was found to increase with refractive index, an effect that is explained by a change in the local optical density of states at the position of the Er^{3+} ions in the film. Radiative and nonradiative components in the decay were separated and the radiative decay rate for Er in bulk SiO_2 was determined to be $54\pm10\,s^{-1}$.

The LDOS for spherical SiO_2 microcavities was cal-

culated for various radii of the sphere. Depending on the sphere radius and the position of the Er ions in the sphere, the radiative decay rate can either be enhanced or inhibited compared to the decay rate in bulk SiO_2. A full determination of the LDOS as a function of sphere diameter revealed that the maxima in the LDOS correspond to the electric-type resonances of the spherical microcavity.

The experimentally obtained value for the decay rate in bulk SiO_2 was used to compare decay rates measured for Er^{3+} implanted in 340-nm-diam SiO_2 colloidal spheres. By index-matching the spheres, a large increase in decay rate from 69 to 101 s^{-1} was observed. The increase can be explained by the calculated increase of the LDOS for a single spherical microcavity.

ACKNOWLEDGMENTS

Dirk Vossen is gratefully acknowledged for the synthesis of the colloidal spheres and SiO_2 layers. The authors would also like to thank Adriaan Tip, Stefan Scheel, and Ad Lagendijk for stimulating discussions. This work is part of the research program of the Foundation for Fundamental Research on Matter (FOM) and was made possible by financial support from the Dutch Foundation of Scientific Research (NWO).

[1] P. Goy, J. M. Raimond, M. Gross, and S. Haroche, Phys. Rev. Lett. **50**, 1903 (1983).
[2] R. G. Hulet, E. S. Hilfer, and D. Kleppner, Phys. Rev. Lett. **55**, 2137 (1985).
[3] M. Suzuki, H. Yokoyama, S. D. Brorson, and E. P. Ippen, Appl. Phys. Lett. **58**, 998 (1991).
[4] A. M. Vredenberg, N. E. J. Hunt, E. F. Schubert, D. C. Jacobson, J. M. Poate, and G. J. Zydzik, Phys. Rev. Lett. **71**, 517 (1993).
[5] M. D. Tocci, M. Scalora, M. J. Bloemer, J. P. Dowling, and C. M. Bowden, Phys. Rev. A **53**, 2799 (1996).
[6] G. L. J. A. Rikken, Phys. Rev. A **51**, 4906 (1995).
[7] R. M. Amos and W. L. Barnes, Phys. Rev. B **55**, 7249 (1997).
[8] K. H. Drexhage, J. Lumin. **1-2**, 693 (1970).
[9] E. Snoeks, A. Lagendijk, and A. Polman, Phys. Rev. Lett. **74**, 2459 (1995).
[10] T. M. Hensen, M. J. A. de Dood, and A. Polman, J. Appl. Phys. **88**, 5142 (2000).
[11] A. J. Campillo, J. D. Eversole, and H.-B. Lin, Phys. Rev. Lett. **67**, 437 (1991).
[12] H.-B. Lin, J. D. Eversole, C. D. Merritt, and A. J. Campillo, Phys. Rev. A **45**, 6756 (1992).
[13] B. Y. Tong, P. K. John, Y. Zhu, Y. S. Liu, S. K. Wong, and W. R. Ware, J. Opt. Soc. Am. B **10**, 356 (1993).
[14] J. Martorell and N. M. Lawandy, Phys. Rev. Lett. **65**, 1877 (1990).
[15] E. P. Petrov, V. N. Bogomolov, I. I. Kalosha, and S. V. Gaponenko, Phys. Rev. Lett. **81**, 77 (1998).
[16] M. Megens, J. E. G. J. Wijnhoven, A. Lagendijk, and W. L. Vos, Phys. Rev. A **59**, 4727 (1999).
[17] R. Sprik, B. A. van Tiggelen, and A. Lagendijk, Europhys. Lett. **35**, 265 (1996).
[18] R. J. Glauber and M. Lewenstein, Phys. Rev. A **43**, 467 (1991).
[19] A. Tip, Phys. Rev. A **56**, 5022 (1997).
[20] K. Khosravi and R. Loudon, Proc. R. Soc. London, Ser. A **433**, 337 (1991).
[21] H. Khosravi and R. Loudon, Proc. R. Soc. London, Ser. A **436**, 373 (1992).
[22] H. P. Urbach and G. L. J. A. Rikken, Phys. Rev. A **57**, 3913 (1998).
[23] A. Moroz, Europhys. Lett. **46**, 419 (1999).
[24] L. Knöll, S. Scheel, and D.-G. Welsch, *QED in Dispersing and Absorbing Media*, in *Coherence and Statistics of Photons and Atoms*, edited by J. Peřina (Wiley, New York, 2001).
[25] L. H. Slooff, M. J. A. de Dood, A. van Blaaderen, and A. Polman, Appl. Phys. Lett. **76**, 3682 (2000).
[26] A. Polman, J. Appl. Phys. **82**, 1 (1997).
[27] A. P. Philipse and A. J. Vrij, J. Chem. Phys. **10**, 5634 (1987).
[28] G. H. Bogush, M. A. Tracy, and C. F. Zukoski IV, J. Non-Cryst. Solids **104**, 95 (1988).
[29] A. van Blaaderen, J. van Geest, and A. Vrij, J. Colloid Interface Sci. **2**, 481 (1992).
[30] S.-L. Chen, P. Dong, G.-H. Yang, and J.-J. Yang, J. Colloid Interface Sci. **189**, 268 (1997).
[31] D. L. J. Vossen, M. J. A. de Dood, T. van Dillen, T. Zijlstra, E. van der Drift, A. Polman, and A. van Blaaderen, Adv. Mater. **12**, 1434 (2000).
[32] A. Polman, D. C. Jacobson, D. J. Eaglesham, R. C. Kistler, and J. M. Poate, J. Appl. Phys. **70**, 3778 (1991).
[33] This assumption can be justified by an analysis of measured changes in the radiative decay rate of Er ions in sodalime silicate glass incorporated at two different depths [9], comparable to the depth scales in our experiments. In these experiments, the changes in lifetime were fully described by changes in the LDOS.
[34] Using spectroscopic ellipsometry measurements, we found that indices at 1.5 μm are typically 0.01–0.02 lower both for SiO_2 and the liquids.
[35] W. J. Miniscalco, J. Lightwave Technol. **9**, 234 (1991).
[36] G. Stein and E. Würzberg, J. Chem. Phys. **62**, 208 (1975).
[37] V. L. Ermolaev and E. B. Sveshnikova, Russ. Chem. Rev. **63**, 905 (1994).
[38] A. Tip, J. Math. Phys. **38**, 3545 (1997).
[39] D. S. Jones, *Acoustic and Electromagnetic Waves* (Oxford University Press, Oxford, 1986).
[40] M. S. Tomaš, Phys. Rev. A **51**, 2545 (1995).
[41] The LDOS enhancement close to the sphere surface is given by $1+6(\varepsilon_s-\varepsilon_h)/(\varepsilon_s+\varepsilon_h)$, with ε_s and ε_h the dielectric constant of the sphere and host, respectively; see, for instance, J. D. Jackson, *Classical Electrodynamics* (Wiley, New York, 1975).
[42] H. C. Chow and R. C. Powell, Phys. Rev. B **21**, 3785 (1980).
[43] P. A. Bobbert and J. Vlieger, Physica A **137**, 209 (1986).